Applied Surface Science 276 (2013) 328–332

Contents lists available at SciVerse ScienceDirect

Applied Surface Science

journal homepage: www.elsevier.com/locate/apsusc

Catalytic combustion of methane on $La_{1-x}Ce_xFeO_3$ oxides

Xian-Ping Xiang, Lei-Hong Zhao*, Bo-Tao Teng, Jia-Jian Lang, Xin Hu, Tie Li, Yi-An Fang, Meng-Fei Luo, Jian-Jun Lin*

Institute of Physical Chemistry, Zhejiang Normal University, Jinhua 321004, China

ARTICLE INFO

Article history:
Received 28 November 2012
Received in revised form 14 March 2013
Accepted 16 March 2013
Available online 21 March 2013

Keywords:
$LaFeO_3$
Methane oxidation
Perovskite
DFT

ABSTRACT

A series of $La_{1-x}Ce_xFeO_3$ (x = 0–0.5) perovskite oxides were prepared by a sol–gel method. X-ray diffraction spectrometer (XRD), BET surface area measurements, scanning electron microscopy (SEM) images, and temperature-programmed reduction (TPR) were used to characterize their physical structures and redox properties. Catalytic methane combustion tests for $La_{1-x}Ce_xFeO_3$ (x = 0–0.5) perovskite oxides show that the activity of $LaFeO_3$ was highly improved due to the introduction of Ce in the A-site of the perovskite catalysts. Among all the catalysts, $La_{0.7}Ce_{0.3}FeO_3$ has the maximum oxidative performance with the corresponding T_{90} as low as 510 °C. Combining with density functional theory calculation, it was suggested that the electrons of Fe ions increase in $La_{0.875}Ce_{0.125}FeO_3$ due to the introduction of Ce^{4+} ion, which leads to stronger interactions with adsorbed O_2. Correspondingly, the adsorption energy of O_2 on $La_{0.875}Ce_{0.125}FeO_3$ increases and the O—O bond is activated. Thus, the Ce doped perovskite has higher oxidative activity than pure $LaFeO_3$.

1. Introduction

Catalytic combustion of methane has received much attention due to its increasing application in environment-friendly fuel [1]. To eliminate methane in tail gas of natural gas automobile, a catalyst with high performance is necessary. Noble metals supported on oxide carriers are the good choices [2,3]. Whereas with the depleting resources and increasing prices of noble metals, a series of non-noble metal-based catalysts have been explored. The perovskite-type oxides (ABO_3) are the most promising alternatives to partially substitute the noble metal-based catalysts due to their unique structures and high performances in catalytic oxidation [4–6]. A perovskite-type oxide has an ABO_3 crystal structure wherein A-site cation with a large ionic radius has 12 coordination to oxygen atoms, and B-site cation with a smaller ionic radius has six coordination. The most outstanding advantage of perovskite oxides is their wide variety of composition and constituent elements with the basic structure unchanged, which make them widely apply into electronic and catalytic materials [7,8].

Since the first report in catalytic hydrocarbon combustion by Libby [9], a series of $LaBO_3$ has been extensively studied as catalysts to eliminate automobile exhaust. Blasin-Aubé et al. [10] studied the catalytic oxidation of a variety of VOCs with different functional groups over $La_{0.8}Sr_{0.2}MnO_{3+x}$, and found that the total oxidation temperature was below 623 K. The acetone, isopropanol, and benzene oxidation performances of $LaMnO_3$ and $LaCoO_3$ catalysts were systematically compared by Spinicci et al. [11] Based on the investigation of $LaMO_3$ (M = Mn, Fe, Cu, Co, Ni, Cr) oxides in methane combustion, Arai et al. [12] found that the partially cation-substituted La—Fe, La—Mn, and La—Co oxide systems showed high oxidation activities. An excellent review by Tejuca et al. [6] pointed out that B-site was the key factor to catalyst for ABO_3. For $LaMO_3$, the oxidative (Cr, Mn) and reductive (Co, Ni, and Rh) nonstoichiometry perovskites were correlated with its catalytic performance. Using density functional theory, Liu et al. [13] suggested that the band gap is decreased by the doping Mg in $LaFe_{1-x}Mg_xO_3$, which increases the adsorption energy of O_2. Compared with extensive studies for the effects of different metal cations in B-site of $LaBO_3$ on VOCs combustion, the effects of cations in A-site of $LaBO_3$ have seldom been reported. Recently, Pecchi et al. [14] reported that perovskite-type $La_{1-x}Ca_xFeO_3$ had the highest catalytic activity for methane combustion when x is equal to 0.4. They ascribed the high activity of $La_{1-x}Ca_xFeO_3$ to the formation of Fe^{4+} and oxygen vacancies. Does this conclusion still work for the cation with high valence in A-site, such as Ce^{4+} ion?

To explore this question, the $La_{1-x}Ce_xFeO_3$ compounds, in which the A-site La atom was partially substituted by Ce atom were systematically studied in the present work. Using a sol–gel method, a series of perovskite-type $La_{1-x}Ce_xFeO_3$ with different x ratio were synthesized. Then, the physical structures and chemical properties were characterized by X-ray diffraction spectrometer (XRD), BET surface area measurements, scanning electron microscopy (SEM) images, and temperature-programmed reduction (TPR). The

* Corresponding authors. Tel.: +86 579 82282234; fax: +86 579 82282595.
E-mail addresses: zlh@zjnu.cn, zhaoleihong@163.com (L.-H. Zhao), linjj@zjnu.cn (J.-J. Lin).

0169-4332/$ – see front matter © 2013 Elsevier B.V. All rights reserved.
http://dx.doi.org/10.1016/j.apsusc.2013.03.091

corresponding performances of catalytic combustion of methane for $La_{1-x}Ce_xFeO_3$ catalysts were evaluated.

2. Experimental

2.1. Catalyst preparation

The catalysts were prepared by a sol–gel method, which is chosen here due to its easiness to operate, relatively low calcination temperature combined with small and uniform sizes of as-synthesized products. $Ce(NO_3)_3{\cdot}6H_2O$ and $La(NO_3)_3{\cdot}5H_2O$ with different molar ratios of $x/(1-x)$ (x = 0, 0.1, 0.2, 0.3, 0.4, and 0.5) were dissolved in deionized water, and mixed with a $Fe(NO_3)_3$ solution at a constant composition level. To this solution, the citric acid with a acid/(Ce + La) molar ratio of 1.5/1 was added. After fully mixing, a NH_4OH solution was introduced and stirred at 80 °C in a water bath for 30 min. Then the mixture was dried at 200 °C for 1 h in an oven, followed by calcination at 750 °C for 4 h in a muffle furnace. The final mixed oxides were composed of $(1-x)$La/xCe/Fe (x = 0, 0.1, 0.2, 0.3, 0.4, and 0.5) in molar ratio, respectively.

2.2. Catalyst characterization

X-ray diffraction (XRD) patterns were collected on a PANalytical X'Pert PRO MPD powder diffractometer using Cu Kα radiation (λ = 0.1542 nm, 40 kV/40 mA). The patterns were collected in a 2θ range from 10° to 110°. The lattice parameter and the mean crystallite size were determined by the Rietveld method using JADE 6.5 software. Brunauner–Emmett–Teller (BET) surface areas were measured by N_2 adsorption on a Quantachrome Autosorb-1 (Quantachrome Instruments). SEM micrographs were recorded by the field emission scanning electron microscope (Hitachi S-4800).

Hydrogen temperature-programmed reduction (H_2-TPR) measurements were performed in an atmospheric quartz tube flow reactor with a thermal conductivity detector (TCD). Under a flow of 30 ml min^{-1} 5 vol.% H_2/N_2, the samples were heated to 900 °C at a rate of 10 °C/min.

2.3. Catalyst testing

The catalytic combustion of methane was carried out in a quartz tubular (i.d. = 6 mm) fixed-bed reactor under atmospheric pressure. 200 mg of the catalyst (150–180 μm) was loaded in the reactor, and the reaction temperature was detected by a thermocouple placed in the middle of the catalyst bed. The flow rate of gas reactant was 40 ml min^{-1}, corresponding to a space velocity of 12,000 ml g_{cat}^{-1} h^{-1}. The reactant is a gas mixture of 0.5 vol.% CH_4, 3 vol.% O_2 and 96.5 vol.% N_2. The CH_4 concentrations before and after oxidation were analyzed using a Shimadzu GC-14 gas chromatograph equipped with a FID detector and a Supelcowax-10 (30 m × 0.25 mm × 0.25 μm) column. Conversion of CH_4 was defined as the following equation:

$$CH_4 \text{ conversion} = \frac{[CH_4]_{in} - [CH_4]_{out}}{[CH_4]_{in}} \times 100\%$$

where $[CH_4]_{in}$ and $[CH_4]_{out}$ are the methane concentration in the feed gas and product, respectively.

3. Result

3.1. Structural characterization

As shown in Fig. 1, the XRD diffractograms of $La_{1-x}Ce_xFeO_3$ perovskite with different Ce/La ratio calcined at 750 °C, the characteristic diffraction peaks (2θ = 32.4°, 46.6°, and 57.9°) have been observed corresponding to the orthorhombic structure of $LaFeO_3$ with a space group of *Pnma*, N.62. When x is 0.1, no XRD diffraction peaks of ceria are detected, indicating that the doped Ce atoms might have embodied into the $LaFeO_3$ lattice to form a solid solution. When x increases to 0.2, small diffraction peaks of cubic ceria appear. With the increase of x, the peak intensity of ceria increases, and the peak intensity of $LaFeO_3$ decreases, simultaneously. This implies the formation of ceria phase and its separation from perovskite oxide. Similar phase separation has been observed for the $La_{1-x}Ca_xFeO_3$ perovskite when x is higher than 0.4 [14]. Although no Fe_2O_3 peaks were detected in the XRD diffraction spectroscopy, Fe_2O_3 is proposed to be separated from perovskite oxides accompanying with the separation of CeO_2 phase, which will be proved by the following H_2-TPR profiles.

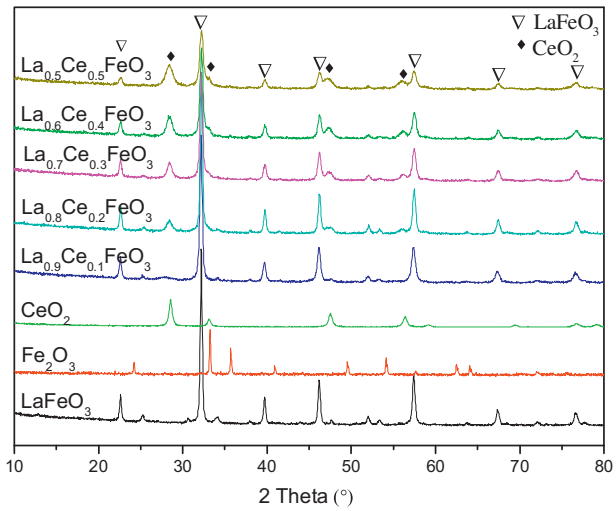

Fig. 1. XRD patterns of $La_{1-x}Ce_xFeO_3$, CeO_2 and Fe_2O_3 samples.

Table 1 lists the BET surface areas and lattice parameters of $La_{1-x}Ce_xFeO_3$ with different x values. All the catalysts have been calcined at 750 °C. It can be learned from Table 1 that the surface area of $La_{0.9}Ce_{0.1}FeO_3$ is almost the same as that of pure $LaFeO_3$. This might be due to the fact that Ce atoms embody into the A-site without changing the pristine perovskite structure. This is consistent with the above XRD results, of which $La_{0.9}Ce_{0.1}FeO_3$ and $LaFeO_3$ show the same diffraction patterns. With the further increase of x, the surface area of $La_{1-x}Ce_xFeO_3$ firstly increases from 9.7 m^2/g in $LaFeO_3$ to 13.3 m^2/g when x = 0.2 and reaches 17.7 m^2/g when x = 0.3, then slightly decreases to about 15 m^2/g when x equals to 0.4 and 0.5. The increase in surface area of $La_{0.8}Ce_{0.2}FeO_3$ might be caused by the separation of CeO_2 and Fe_2O_3 nano-particles from perovskite oxide. When x is larger than 0.3, the separated oxide particles might begin to grow slightly and lead to the corresponding decrease in surface area. This finding is consistent with the XRD results i.e. the intensity of diffraction peak increases with increasing x in $La_{1-x}Ce_xFeO_3$ and will be further verified by SEM measurements.

Table 1
BET surface areas and lattice parameters $La_{1-x}Ce_xFeO_3$.

Catalysts	S_{BET}/m^2/g	Lattice constants/Å			V/Å^3	Crystallite size/nm
		a	b	c		
$LaFeO_3$	9.7	5.553	7.867	5.563	243.02	37.0
$La_{0.9}Ce_{0.1}FeO_3$	9.1	5.567	7.855	5.533	241.95	32.6
$La_{0.8}Ce_{0.2}FeO_3$	13.3	5.565	7.855	5.556	242.87	33.6
$La_{0.7}Ce_{0.3}FeO_3$	17.7	5.567	7.855	5.533	241.95	30.0
$La_{0.6}Ce_{0.4}FeO_3$	14.5	5.567	7.855	5.533	241.95	28.4
$La_{0.5}Ce_{0.5}FeO_3$	15.0	5.567	7.855	5.533	241.95	25.2

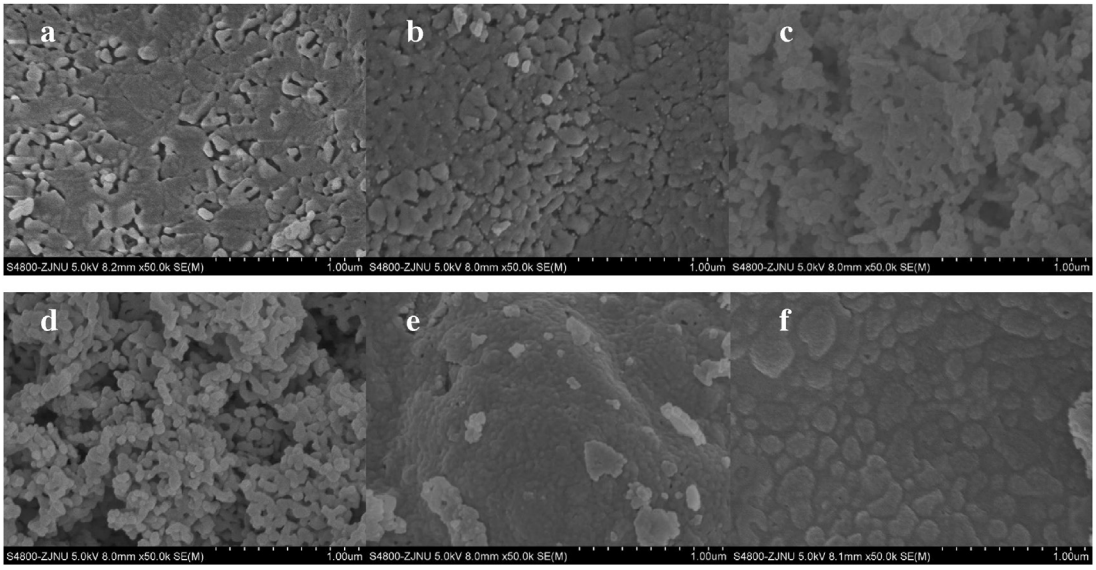

Fig. 2. SEM images of $La_{1-x}Ce_xFeO_3$ samples. (a)–(f) corresponds to the x value of 0, 0.1, 0.2, 0.3, 0.4, and 0.5, respectively.

According to the SEM images of $La_{1-x}Ce_xFeO_3$ (Fig. 2), the surface morphology of $LaFeO_3$ and $La_{0.9}Ce_{0.1}O_3$ is similar. However, the small branch-shape structures were observed when x increases to 0.2 and 0.3, which might be attributed to the phase separation of ceria and Fe_2O_3 from perovskite oxide. When x is up to 0.4 and 0.5, relatively big nano-particles were obtained due to the increase of separated ceria and Fe_2O_3. The SEM results support the above analysis results of XRD and BET surface area.

The redox properties of $La_{1-x}Ce_xFeO_3$ with different molar ratios of La/Ce were studied by H_2-TPR, as shown in Fig. 3. It can be seen from Fig. 3 that a broad reduction peak is observed for pure $LaFeO_3$ at c.a. 500 °C; while a shoulder peak appears at 430 °C for $La_{0.9}Ce_{0.1}O_3$, which might be ascribed to the effects of doped Ce atoms. When x increases to 0.2, a new peak is observed at 390 °C for $La_{0.8}Ce_{0.2}O_3$, which is attributed to the reduction of Fe_2O_3. For $La_{0.7}Ce_{0.3}O_3$, the peak area at 390 °C increases greatly compared with $La_{1-x}Ce_xFeO_3$ (x = 0, 0.1 and 0.2). Simultaneously, a new β peak at 500 °C appears, which is attributed to the reduction of small ceria nano-particles separated from perovskite oxide based on the above XRD and nitrogen adsorption results. With the further increase of x, the two reduction peak areas increase and peak position slightly shifts toward high temperature due to the enhanced size of oxide particles.

3.2. Catalytic activity

Fig. 4 shows the catalytic activities of $La_{1-x}Ce_xFeO_3$, CeO_2 and Fe_2O_3 samples for methane combustion. It can be seen from Fig. 4 that pure ceria has a low CH_4 combustion activity, of which the temperatures of CH_4 conversion at 10% and 50% (T_{10} and T_{50}) are 450 and 560 °C, respectively; the oxidative activity of $LaFeO_3$ is higher than that of ceria at low temperature with T_{10} of 390 °C, while the T_{10} and T_{50} of Fe_2O_3 are 410 and 520 °C, respectively. When a small quantity of Ce atom was doped into $LaFeO_3$ to form the solid solution, $La_{0.9}Ce_{0.1}O_3$, the perovskite sample's reactivity improves greatly with the reduction of T_{10} and T_{50} to 360 and 460 °C, respectively. With the increase of x, the oxidative activity of methane increases slightly first and reaches the maximum when x = 0.3. The corresponding T_{90} is as low as 510 °C. However, when x is further raised to 0.4 and 0.5, its activity of CH_4 combustion decreases, correspondingly.

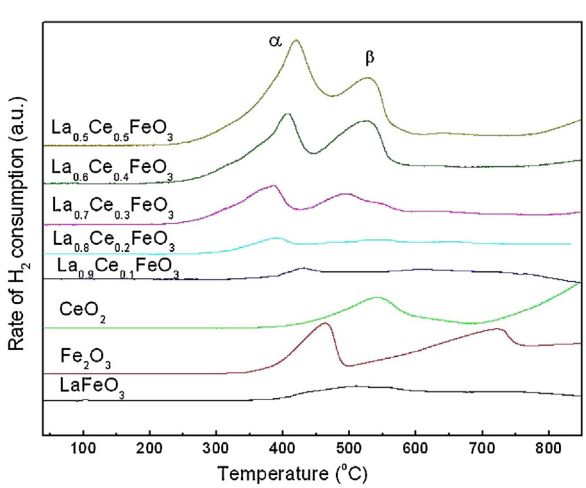

Fig. 3. H_2-TPR profiles of $La_{1-x}Ce_xFeO_3$, CeO_2 and Fe_2O_3 samples powder samples.

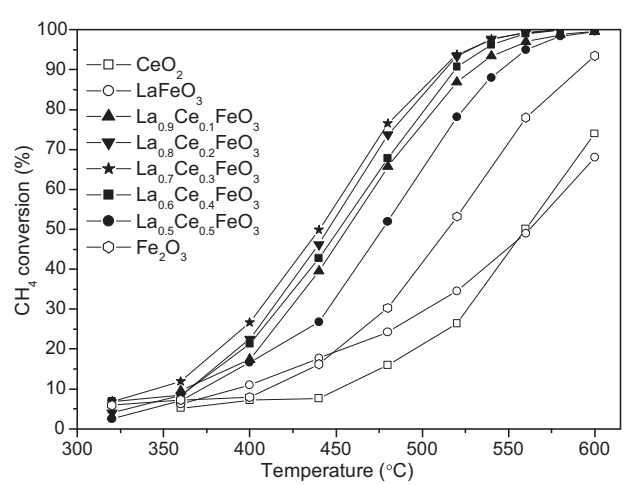

Fig. 4. Catalytic activities of $La_{1-x}Ce_xFeO_3$, CeO_2 and Fe_2O_3 samples for methane combustion.

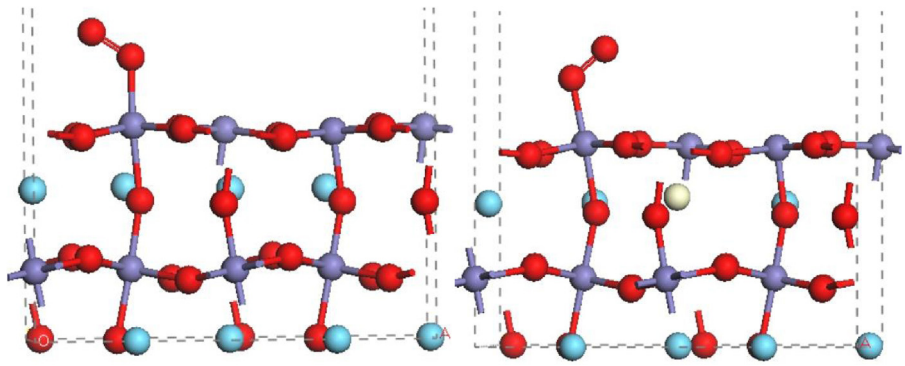

Fig. 5. O_2 adsorbed on $LaFeO_3$(0 1 0) and $La_{0.875}Ce_{0.125}FeO_3$(0 1 0) surfaces. : La, : Ce, : Fe, : O.

Table 2
Bader charges of Fe, Ce and O_2 on $LaFeO_3$(0 1 0) and $La_{0.875}Ce_{0.125}FeO_3$(0 1 0).

Atomic type	$LaFeO_3$	$La_{0.875}Ce_{0.125}FeO_3$	$O_2/LaFeO_3$	$O_2/La_{0.875}Ce_{0.125}FeO_3$
Fe_{total}	13.34	13.14	13.47	13.41
Ce	–	2.20	–	2.18
$O_{2,ads}$	–	–	−0.43	−0.39

Note: Bader charge of $Ce^{4+}(CeO_2)$ and $Ce^{3+}(Ce_2O_3)$ ions are 2.29 and 1.86 calculated herein, respectively.

4. Discussion

The great improvement of CH_4 combustion for $La_{0.9}Ce_{0.1}FeO_3$ might be due to the doping effects of Ce. When Ce^{4+} ion substitutes the position of La^{3+} in A-site, it might cause the charge imbalance of perovskite, which was also observed in $La_{1-x}Ca_xFeO_3$ and $La_{1-x}Sr_xFeO_3$ [10,14]. Until now, it was widely accepted that the doped metals with a lower valence (Ca^{2+} or Sr^{2+}) compared with La^{3+} might lead to more oxygen vacancies in the perovskite oxides [1,8]. Then, O_2 might fill into the surface vacancies and be activated to form superoxide or peroxide species [15]. Correspondingly, the activated oxygen species take part into the successive oxidative reactions. However, the doped Ce^{4+} ion is quite different from the metal ions with low valence then how does it affect the oxidative performances of $La_{1-x}Ce_xFeO_3$?

To explore the possible effects of doped Ce ion in $La_{1-x}Ce_xFeO_3$, we calculate O_2 adsorption behaviors on the $LaFeO_3$(0 1 0) and $La_{0.875}Ce_{0.125}FeO_3$(0 1 0) surfaces using density functional theory method. The corresponding optimized structures of O_2 were shown in Fig. 5. Detailed descriptions of theoretical model and method can be seen in the supplementary materials.

As shown in Fig. 5(a), O_2 stands on the top site of surface Fe for $LaFeO_3$(0 1 0) to form a Fe—O bond with the length of 1.917 Å. The O—O bond of adsorbed O_2 is elongated to 1.282 Å, which is longer than that of free O_2 (1.21 Å). The corresponding adsorption energy is −0.42 eV, which is consistent with the value reported in the literature [13,16]. Similar structure was also obtained for O_2 on $La_{0.875}Ce_{0.125}FeO_3$(0 1 0) surface. Its Fe—O bond length is 1.889 Å, which is slightly shorter that on $LaFeO_3$. While the O—O bond (1.289 Å) is slightly longer than on $LaFeO_3$, indicating relatively strong interactions between O_2 and the doped perovskite oxides. This conclusion is further proved by the adsorption energy of O_2 on $La_{0.875}Ce_{0.125}FeO_3$(0 1 0) (−0.69 eV), which is higher than that on $LaFeO_3$.

To further understand the effects of doped Ce ion, the bader charges of Ce, O_2 and the sum of Fe ions were listed in Table 2. The total charges of La and O ions almost did not change no matter with and without Ce doped and were not listed herein. As seen in Table 2, the charge of Ce ion in $La_{0.875}Ce_{0.125}FeO_3$ is 2.20, which is much higher than that of Ce^{3+}(1.86) and approaches to Ce^{4+}(2.29) ion, indicating that the doped Ce ion approximates Ce^{4+}. Due to the introduction of Ce^{4+} ion, the total charge of Fe ions decreases by 0.2 to keep $La_{0.875}Ce_{0.125}FeO_3$ electronic neutral. Therefore, the electrons of Fe ions increase and stronger interactions occur between Fe and the adsorbed O_2. Correspondingly, O_2 is activated and might lead to higher oxidative reactivity on $La_{1-x}Ce_xFeO_3$ than on pure $LaFeO_3$, which is observed by the catalytic test for methane combustion in the present work.

5. Conclusion

A series of $La_{1-x}Ce_xFeO_3$ (x = 0–0.5) perovskite oxides were prepared, characterized and tested by methane catalytic combustion reaction. Our results show that the activity of $LaFeO_3$ was highly improved due to the introduction of Ce in the A-site of the perovskite catalysts, and reaches the maximum for $La_{0.7}Ce_{0.3}FeO_3$. The corresponding T_{90} is as low as 510 °C. Density functional theory calculation suggests that the electrons of Fe ions increase in $La_{0.875}Ce_{0.125}FeO_3$ due to the introduction of Ce^{4+} ion, and leads to stronger interactions with $O_{2,ads}$. Therefore, the adsorption energy of O_2 on $La_{0.875}Ce_{0.125}FeO_3$ increases and the O—O bond is activated. Correspondingly, the Ce doped perovskites have higher oxidative activity than pure $LaFeO_3$.

Acknowledgements

This work was supported by the National Natural Science Foundation of China (Grant No. 20903081), and the Natural Foundation of Zhejiang Province, China (Grant No. Y407163).

Appendix A. Supplementary data

Supplementary data associated with this article can be found, in the online version, at http://dx.doi.org/10.1016/j.apsusc.2013.03.091.

References

[1] C.-H. Wang, C.-L. Chen, H.-S. Weng, Surface properties and catalytic performance of $La_{1-x}Sr_xFeO_3$ perovskite-type oxides for methane combustion, Chemosphere 57 (2004) 1131–1138.
[2] R. Burch, P.K. Loader, Investigation of Pt/Al_2O_3 and Pd/Al_2O_3 catalysts for the combustion of methane at low concentrations, Applied Catalysis B: Environmental 5 (1994) 149–164.
[3] L. Meng, J.-J. Lin, Z.-Y. Pu, L.-F. Luo, A.-P. Jia, W.-X. Huang, M.-F. Luo, J.-Q. Lu, Identification of active sites for CO and CH_4 oxidation over $PdO/Ce_{1-x}Pd_xO_{2-\delta}$ catalysts, Applied Catalysis B: Environmental 119 (2012) 117–122.
[4] H. Tanaka, M. Misono, Advances in designing perovskite catalysts, Current Opinion in Solid State and Materials Science 5 (2001) 381–387.
[5] Z. Zhong, K. Chen, Y. Ji, Q. Yan, Methane combustion over B-site partially substituted perovskite-type $LaFeO_3$ prepared by sol–gel method, Applied Catalysis A: General 156 (1997) 29–41.

[6] L.G. Tejuca, J.L.G. Fierro, J.M.D. Tascón, Structure and reactivity of perovskite-type oxides, Advances in Catalysis 36 (1989) 237–328.
[7] T. Setoguchi, M. Sawano, K. Eguchi, H. Arai, Application of the stabilized zirconia thin film prepared by spray pyrolysis method to SOFC, Solid State Ionics 40–41 (1990) 502–505.
[8] T. Nitadori, M. Misono, Catalytic properties of $La_{1-x}A_xFeO_3$(A = Sr, Ce) and $La_{1-x}Ce_xCoO_3$, Journal of Catalysis 93 (1985) 459–466.
[9] W. Libby, Promising catalyst for auto exhaust, Science 171 (1971) 499–500.
[10] V. Blasin-Aubé, J. Belkouch, L. Monceaux, General study of catalytic oxidation of various VOCs over $La_{0.8}Sr_{0.2}MnO_{3+x}$ perovskite catalyst – influence of mixture, Applied Catalysis B: Environmental 43 (2003) 175–186.
[11] R. Spinicci, M. Faticanti, P. Marini, S. De Rossi, P. Porta, Catalytic activity of $LaMnO_3$ and $LaCoO_3$ perovskites towards VOCs combustion, Journal of Molecular Catalysis A: Chemical 197 (2003) 147–155.
[12] H. Arai, T. Yamada, K. Eguchi, T. Seiyama, Catalytic combustion of methane over various perovskite-type oxides, Applied Catalysis 26 (1986) 265–276.
[13] X. Liu, B. Cheng, J. Hu, H. Qin, Study on adsorption of O_2 on $LaFe_{1-x}Mg_xO_3$ (0 1 0) surface by density function theory calculation, Applied Surface Science 258 (2012) 8678–8682.
[14] G. Pecchi, M.G. Jiliberto, A. Buljan, E.J. Delgado, Relation between defects and catalytic activity of calcium doped $LaFeO_3$ perovskite, Solid State Ionics 187 (2011) 27–32.
[15] Y. Zhao, B.-T. Teng, X.-D. Wen, Y. Zhao, Q.-P. Chen, L.-H. Zhao, M.-F. Luo, Superoxide and peroxide species on CeO_2(1 1 1), and their oxidation roles, Journal of Physical Chemistry C 116 (2012) 15986–15991.
[16] X. Liu, J. Hu, B. Cheng, H. Qin, M. Zhao, C. Yang, First-principles study of O_2 adsorption on the $LaFeO_3$ (0 1 0) surface, Sensors and Actuators B: Chemical 139 (2009) 520–526.